Electrically Programmable Bistable Capacitor for High-Frequency Applications Based on Charge Storage at the $(Ba,Sr)TiO_3/Al_2O_3$ Interface

Shunyi Li, Yuliang Zheng, Rolf Jakoby, and Andreas Klein*

Hysteresis is induced in paraelectric $(Ba,Sr)TiO_3$ (BST) thin-film capacitors by inserting an Al_2O_3 barrier layer of a few nanometers in thickness between the BST layer and the electrode. The observed hysteresis is explained by ambipolar charge carrier injection through the Al_2O_3 layer and charge storage at the BST/Al_2O_3 interface. The magnitude of the hysteresis can be directly adjusted by manipulating the thickness ratio between BST and Al_2O_3. Taking into account the low loss of $(Ba,Sr)TiO_3$ capacitors, the observed switching and retention characteristics are suitable for application as non-volatile programmable high-frequency devices, e.g., in radio-frequency identification.

1. Introduction

In the last decades the applications of $(Ba,Sr)TiO_3$ (BST) are mainly focused on tunable microwave components,[1] and ferroelectric random access memories,[2] since BST exhibits a strongly field dependent dielectric constant and a low dielectric loss in its paraelectric phase, which is essential for high-frequency applications. The polarization hysteresis in the ferroelectric phase for higher Ba content enables non-volatile binary data storage. A promising new memory concept based on resistive switching,[3] has been recently demonstrated by using perovskite oxides,[4] which opens a new field for non-volatile memory technologies. However, up to now there exists no direct combination of microwave and memory functionalities. The tunable capacitors built on paraelectric materials have no intrinsic memory function and therefore rely on external peripherals to store their operation point. On the other hand, the memories based on ferroelectricity or resistive switching are not suitable for high-frequency applications due to the high insertion loss and frequency dispersion of ferroelectric materials as well as the complexities for circuitry integration.

A stable hysteresis with highly distinguishable states depending on the history of the device is considered as one of the essential requirements for the binary data storage. There have been a number of observations of hysteretic behaviors reported in paraelectric BST thin films, which have been attributed to lattice stress[5] or intrinsic charged defects.[6] But this kind of hysteresis is normally very weak and depends strongly on substrates, deposition methods and deposition conditions. Since the existence of the hysteresis is due to intrinsic mechanisms, the hysteresis cannot be easily adjusted at will and is therefore not applicable for memory purpose.

In the present work, we demonstrate a pronounced hysteresis in non-ferroelectric BST thin film capacitors induced by the insertion of a thin Al_2O_3 layer between BST and the electrode. Al_2O_3 layers also strongly affect the hysteresis of ferroelectric $Pb(Zr,Ti)O_3$ and $BiFeO_3$.[12] The hysteresis reported here differs from these observations as the $(Ba,Sr)TiO_3$ layers are not ferroelectric. The high-frequency insertion losses are even reduced by the Al_2O_3 layer. Detailed investigations of the *CV* (capacitance-voltage) and *Ct* (capacitance-time) characteristics will be presented, showing a high flexibility for hysteresis manipulation as well as good switching and retention properties. A mechanism based on quantum mechanical tunneling and interface charge storage is proposed for explaining the phenomena.

2. Results and Discussion

2.1. Capacitance Hysteresis of BST/Al_2O_3 Capacitors

Figure 1 shows the *CV* characteristics of three $Ba_{0.6}Sr_{0.4}TiO_3$ capacitors with increasing Al_2O_3 thickness. The BST layers were prepared under identical deposition conditions and have nearly the same thickness around 260 nm, determined by ellipsometry. Two of the samples are covered with 2.5 and 10 nm Al_2O_3, respectively. The overall capacitance decreases with increasing thickness of Al_2O_3, which is caused by the lower permittivity of Al_2O_3 compared to BST.[7,8] The bilayer structure can be considered as two capacitors connected in series. All three samples

Dr. S. Li, Prof. A. Klein
Faculty of Materials Science
Surface Science Division
Darmstadt University of Technology
Petersenstr. 32, 64287, Darmstadt, Germany
E-mail: sli@surface.tu-darmstadt.de
Dr. Y. Zheng, Prof. R. Jakoby
Faculty of Electrical Engineering and Information Technology
Institute of Microwave Engineering and Photonics
Darmstadt University of Technology
Merckstr. 25, 64283, Darmstadt, Germany

DOI: 10.1002/adfm.201200405

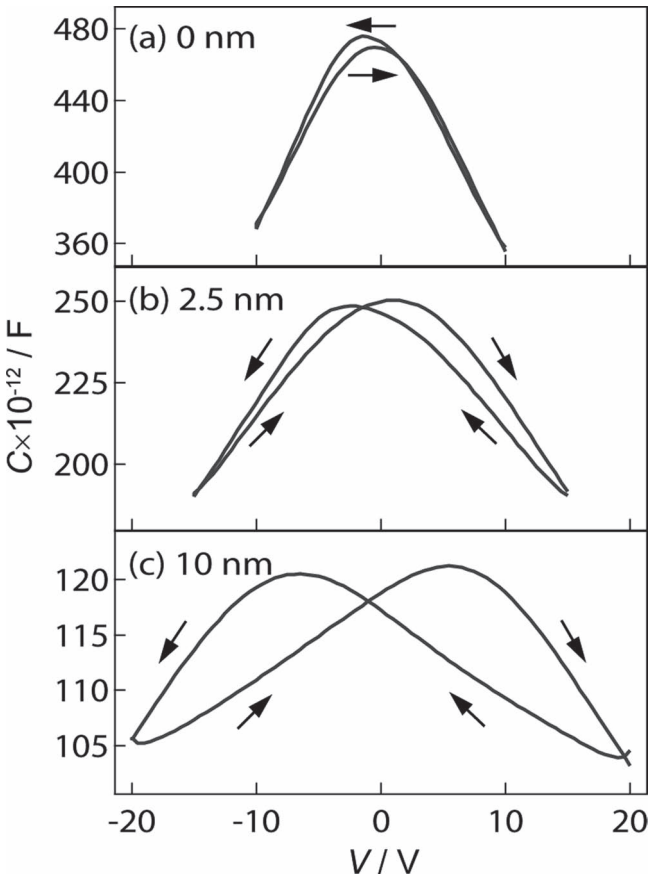

Figure 1. *CV* characteristics of $Ba_{0.6}Sr_{0.4}TiO_3$ capacitors with 0 (a), 2.5 (b), and 10 nm (c) Al_2O_3, at $f = 1$ MHz. The arrows indicate the direction of the voltage sweeps.

exhibit a voltage dependence of capacitance, which is explained by the field dependent permittivity of the BST layer.[9] Dielectric calculations based on a bilayer capacitor model reveal that the permittivity and tunability of BST are not affected by the Al_2O_3 film. The apparent differences in Figure 1 are fully explained by the reduced electric field in BST.

The *CV* curves show a large difference in the hysteretic behavior. The sample without Al_2O_3 shown in Figure 1a has only a weak hysteresis between the forward and backward voltage sweep in the vicinity of $V = 0$. This hysteresis has often been observed in sputtered Pt/BST/Pt capacitors,[7] and has been attributed to different interface properties of the top and bottom contacts:[10] ionized defects such as oxygen vacancies form a space charge layer and act like an interface capacitor. The capacitance of this space charge layer depends on the applied electric field and is determined by the Schottky barrier which is under reverse bias. Since the defect concentration of the two interfaces is different, the overall capacitance exhibits a slight difference depending on the direction of the voltage sweep.[11] Contrasting this very weak hysteresis, a pronounced and symmetric hysteresis is observed for the samples with Al_2O_3, particularly for the sample with 10 nm Al_2O_3. The voltage difference between the two capacitance maxima clearly increases with the thickness of the Al_2O_3 layer, indicating a strong correlation between the hysteresis behavior and the Al_2O_3. Since the Al_2O_3 layer is grown on the top of the BST at room temperature, neither the lattice stress nor the defect concentration in BST is expected to be significantly influenced by the Al_2O_3 layer. Thus, the hysteresis is considered to have another origin.

2.2. Origin of the Hysteresis

Similar hysteretic behavior of ferroelectric thin films with Al_2O_3 layer has been reported by Lee, Jiang and coworkers.[12] The hysteresis of the ferroelectric $Pb(Zr,Ti)O_3$ or $BiFeO_3$ films are magnified by the insertion of Al_2O_3 layers, which results in an almost linear increase of the apparent coercive voltage across the thickened Al_2O_3 layer. However, there exists an essential difference to the hysteresis shown in this article. The hysteresis of the BST/Al_2O_3 bilayers is not related to ferroelectricity. In order to confirm this, a series of samples with different Ba/Sr ratios have been prepared, ranging from $SrTiO_3/Al_2O_3$ to $Ba_{0.8}Sr_{0.2}TiO_3/Al_2O_3$. One example is illustrated in Figure 4 (the *CV* measurements of $Ba_{0.8}Sr_{0.2}TiO_3$, $Ba_{0.3}Sr_{0.7}TiO_3$ and $SrTiO_3$ are given in Figure S1 in the Supporting Information). We have mainly chosen those compositions, whose Curie temperatures are below room temperature, so that any ferroelectric origin of the hysteresis can be unambiguously excluded. X-ray diffraction data also confirm the cubic (non-ferroelectric) crystal structure of our BST films. Since the Al_2O_3 layer is grown on the top of the BST, it is not expected to induce ferroelectricity in the BST films. However, independent on the Ba/Sr ratio, all of these samples show a similar hysteresis after the insertion of Al_2O_3 layer.

A schematic illustration of the mechanism proposed as origin of the hysteresis, involving ambipolar charge injection and interface charge storage, is shown in **Figure 2**. The energy

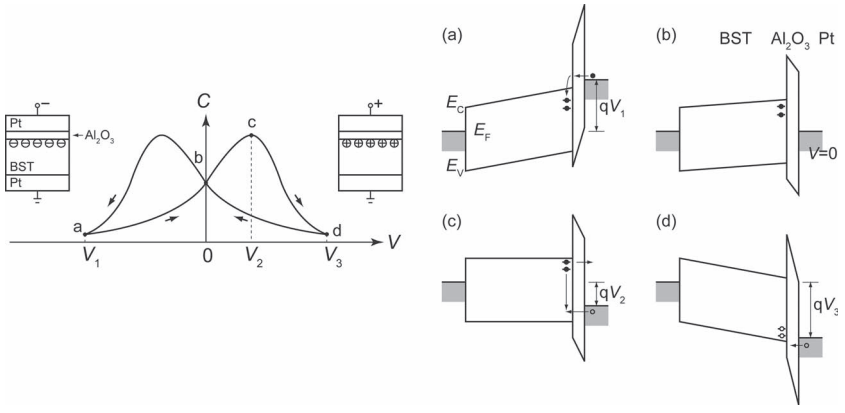

Figure 2. Schematic illustration of the energy band diagram and the ambipolar charge injection for a Pt/BST/Al_2O_3/Pt structure under different DC bias in relation to the *CV* hysteresis. Dots and circles indicate electrons and holes, respectively.

band alignment determined by *in situ* photoelectron spectroscopy was described in the previous work.[13] Because BST and Al_2O_3 have a large difference in the relative permittivity, a significant part of the total applied voltage drops on the Al_2O_3 layer according to the serial-capacitor structure. Therefore the energy bands of the Al_2O_3 and the Fermi level of the Pt electrode shift significantly upwards with respect those of the BST when a negative voltage (V_1) is applied, as indicated in Figure 2a. As soon as the Fermi level of the Pt overlaps with the conduction band of the BST, electrons will be injected into the BST by tunneling through the Al_2O_3 layer. Such tunneling process was confirmed by the current-voltage measurements,[13] and also observed by other authors in similar metal-insulator-semiconductor systems.[14,15] The potential drop on the Al_2O_3 layer depends largely on the thickness ratio of the BST/Al_2O_3 bilayer structure. As long as the Al_2O_3 layer is thin, although the potential drop on Al_2O_3 is relatively low, charge carriers can be injected by direct tunneling. When the barrier layer gets thicker, the portion of the potential drop on Al_2O_3 becomes also larger. This leads to a different mechanism, the Fowler-Nordheim process, where the charge carriers only need to tunnel a triangle potential barrier of the Al_2O_3, which is only a part of its thickness (a simulated band diagram under such condition is provided in Figure S3 in the Supporting Information). Some injected electrons might be trapped at the interface between BST and Al_2O_3 and form a negative charge layer. This interface charge builds up an internal electric field in both layers and will only then be removed or compensated when a positive voltage (V_2) is applied, as shown in Figure 2b and c. At $V = V_2$ the flat-band (zero-field) situation is established in the BST film and therefore the *CV* curve shows a maximum. If the positive voltage is further increased (V_3), the Fermi level of the Pt will be shifted towards the valence band of the BST and a positive interface charge is built up by means of tunneling of holes, as illustrated in Figure 2d. This positive interface charge leads then to a mirrored course of the *CV* curve resulting in the observed hysteresis.

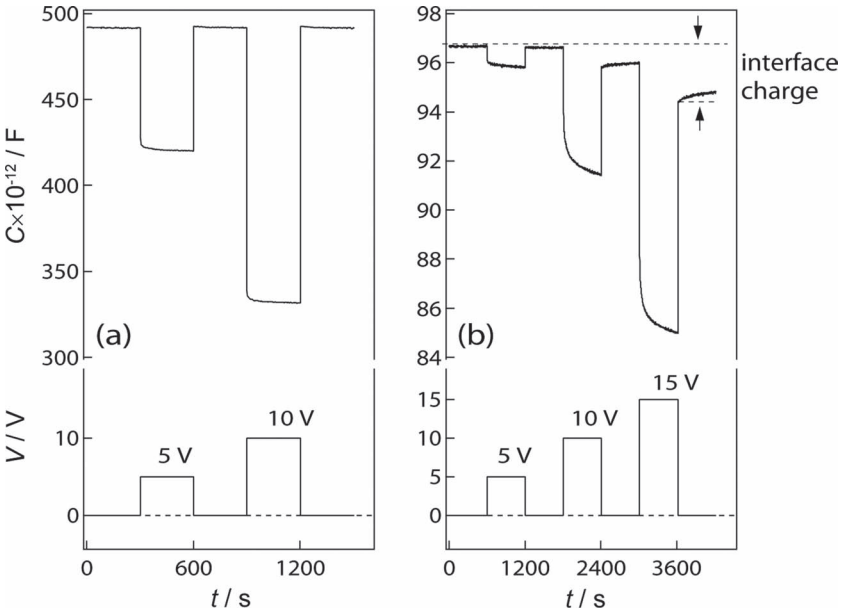

Figure 3. Capacitance vs time of $Ba_{0.6}Sr_{0.4}TiO_3$ capacitors with 0 (a) and 10 nm (b) Al_2O_3 under increasing DC bias at $f = 1$ MHz. The arrows indicate the interface charge which causes the decrease of the capacitance.

The trapping of charge carriers at the interface can be demonstrated by time-dependent capacitance measurements shown in **Figure 3**. With such measurements the capacitance is measured continuously over time while the DC voltage can be simultaneously switched on and off within various time segments. When a voltage is applied, the capacitance shows a sudden drop, which corresponds to the tuning of the relative permittivity of the BST. Compared to the sample having only BST, the sample with 10 nm Al_2O_3 exhibits a distinct transient behavior. After a voltage is applied, the capacitance shows a decrease in addition to the drop although the voltage within this time segment is kept constant. When the voltage is removed, the capacitance does not recover to its original value as the sample without Al_2O_3 does. Similar to the decrease under applied voltage, the capacitance shows a gradual increase with time at $V = 0$. It can be seen in Figure 3b, that the higher the applied voltage, the stronger is the transient behavior. This is related to the field dependence of the tunneling current.[16] According to the model outlined above, the decrease and increase of the capacitance are associated with charging and discharging of the interface (i.e. trapping and detrapping of charge carriers). The difference of the capacitance between the initial and final time segment at $V = 0$ corresponds to the total stored interface charge.

2.3. Dielectric Model and Hysteresis Manipulation

If we consider the interface charge as a homogeneous sheet charge with an area charge density σ, application of Gauss law leads to

$$\epsilon_0\ \epsilon_1\ E_1 + \sigma = \epsilon_0\ \epsilon_2\ E_2 \tag{1}$$

where the indices 1 and 2 represent the BST and Al_2O_3 layer, respectively. After applying a voltage V, the field distribution in the bilayer capacitor is

$$V = E_1 d_1 + E_2 d_2 \tag{2}$$

Combining those two equations above gives the electric field in the individual layer:

$$E_1 = \frac{v - (d_2\sigma)/(\epsilon_0\ \epsilon_2)}{d_1 + (d_2\ \epsilon_1)/\epsilon_2} \tag{3}$$

$$E_2 = \frac{\epsilon_0 \epsilon_1\ E_1 + \sigma}{\epsilon_0\ \epsilon_2} \tag{4}$$

where ε and d are the permittivity and thickness, respectively.

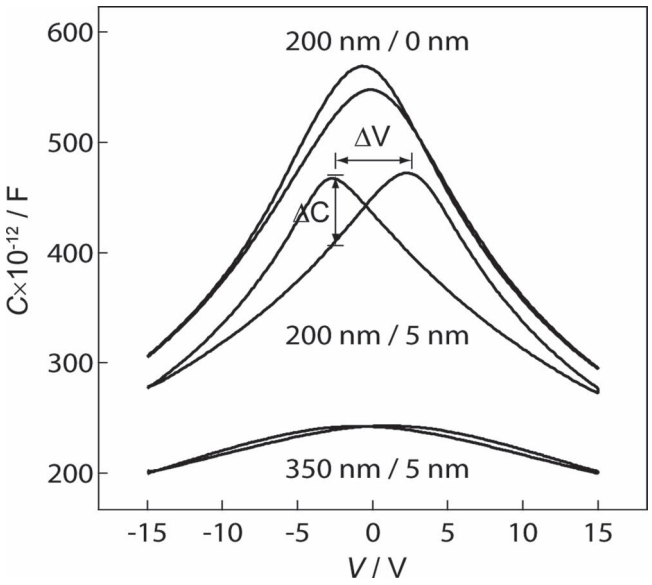

Figure 4. *CV* characteristics of $Ba_{0.1}Sr_{0.9}TiO_3$ capacitors having different BST-to-Al_2O_3 thickness ratio measured at $f = 1$ MHz.

As illustrated in Figure 2b, the *CV* curve reaches the maximum when the electric field in the BST is zero ($E_1 = 0$), leading to the flat-band voltage

$$V_{FB} = \frac{d_2 \sigma}{\epsilon_0 \epsilon_2} \quad (5)$$

The voltage difference of the capacitance maxima ($\Delta V = \pm V_{FB}$) is therefore determined by the thickness of the Al_2O_3 layer (d_2) and by the interface charge density (σ). In principle the hysteresis should become larger with increasing Al_2O_3 layer thickness, which agrees with the observed tendency in Figure 1. However, the thickness of the Al_2O_3 layer also affects the interface charge density σ, because the interface charge density depends on the interplay between the electric field and the tunneling probability. A too thick Al_2O_3 barrier layer is not favorable for inducing hysteresis since the tunneling process will be weakened. On the other hand, for the same thickness of Al_2O_3, the thickness of BST plays also an important role, because the thickness ratio between BST and Al_2O_3 determines the potential distribution in the bilayer capacitor. This effect is demonstrated by another series of capacitors with $Ba_{0.1}Sr_{0.9}TiO_3$, as shown in **Figure 4**. Here the composition with only 10 at% Ba was chosen in order to rule out the ferroelectricity as the origin of the hysteresis, since the Curie temperature of $Ba_{0.1}Sr_{0.9}TiO_3$ is much lower than room temperature.[17] Three different BST-to-Al_2O_3 thickness ratios are applied. The first sample has no Al_2O_3 and serves as the reference. The other two samples contain 200 and 350 nm BST respectively, both covered with 5 nm Al_2O_3. The capacitance also decreases with increasing BST thickness after insertion of the Al_2O_3 layer. The sample without Al_2O_3 exhibits a quite similar *CV* curve as the $Ba_{0.6}Sr_{0.4}TiO_3$ sample shown in Figure 1a. Only a slight difference between the forward and backward sweep, especially at $V = 0$, is observed. In comparison the sample with 200 nm BST and 5 nm Al_2O_3 shows a much pronounced symmetric hysteresis with a voltage difference (ΔV) between the maxima of capacitance of about 5 V. However, the *CV* curve of the sample with 350 nm BST and 5 nm Al_2O_3 exhibits not only a smaller voltage difference between the two capacitance maxima ($\Delta V \approx 3$ V), but also a considerably lower absolute difference in capacitance (ΔC) for forward and reverse voltage sweep compared to the sample with thinner BST.

Both effects can be attributed to a much lower interface charge density, which is caused by the modified potential distribution. According to the serial-capacitor model, the voltage drop on each capacitor depends on the individual capacitance. The potential drop across the Al_2O_3, which is responsible for the charge carrier injection, can be expressed as

$$V_2 = V \frac{C_1}{C_1 + C_2} = V \frac{\epsilon_1}{\epsilon_1 + \epsilon_2 \frac{d_1}{d_2}} \quad (6)$$

Under a certain applied voltage (V) the permittivity values in **Equation 6** are constant. The thicker the BST layer (d_1), the lower is the voltage component on the Al_2O_3 (V_2), which is certainly unfavorable for the tunneling process and leads therefore to a lower interface charge.

2.4. Programmable Bistable Capacitor Operation

The induced *CV* hysteresis based on the BST/Al_2O_3 bilayer structure exhibits a bistability similar to ferroelectric materials, which offers two individual states at the same voltage. The switching characteristics of such a hysteretic capacitor is illustrated exemplarily with a $Ba_{0.1}Sr_{0.9}TiO_3$(200 nm)/Al_2O_3(5 nm) capacitor in **Figure 5**. The operation contains a writing and a reading process, which correspond to a write voltage (V_W) and a read voltage (V_R), respectively. As shown in Figure 5c, the capacitor is preprogrammed with a short DC voltage (V_W = 15 V, $t = 2$ s). The *CV* curve takes then the lower branch of the hysteresis at positive voltages as indicated in Figure 5a and a low capacitance is measured by the read voltage $V_R = 2$ V as shown in Figure 5b. Now if a write voltage with the opposite polarity ($V_W = -15$ V) is applied, the *CV* curve will take the upper branch of the hysteresis and a high capacitance is measured with the same read voltage $V_R = 2$ V. For both cases the capacitance difference is rather constant with time, showing clearly a non-volatile repeatable programmability. The choice of V_W and V_R is in principle arbitrary. However, V_W should be larger than the flat-band voltage (V_{FB}) in order to generate a high charge carrier injection and therefore a high interface charge. V_R should be between 0 and V_{FB} but preferably close to V_{FB} in order to get a large difference between the high and low states. The polarity of V_W and V_R can be arbitrarily correlated since the hysteresis is largely symmetric.

The stability of the charge storage is crucial for the application as passive high-frequency non-volatile devices. The interface charge can disappear gradually through back tunneling or recombination. The retention property of the BST/Al_2O_3 capacitor was characterized by the *Ct* measurement with an extended time scale, as demonstrated in **Figure 6**. For such measurements the capacitor is preprogrammed with ±15 V according to the high and low states respectively at the beginning, and

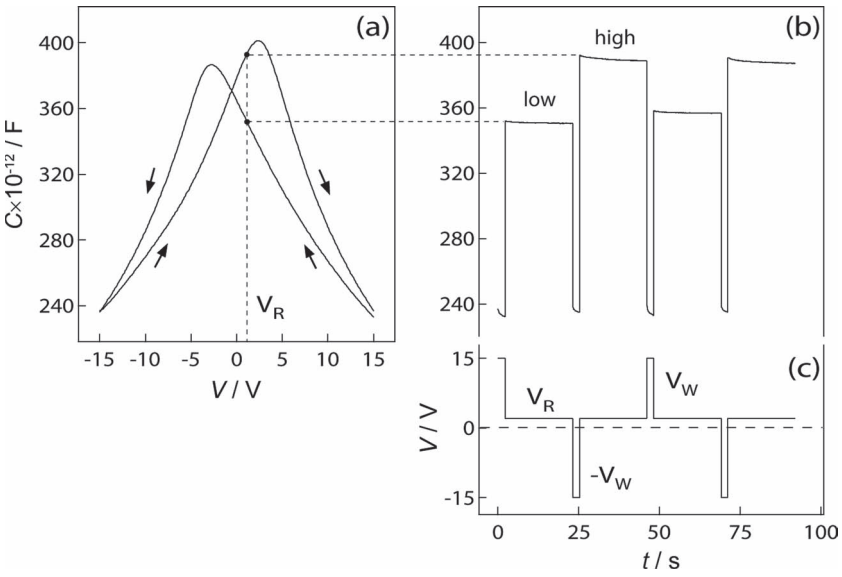

Figure 5. *CV* (a), *Ct* (b) characteristics of a $Ba_{0.1}Sr_{0.9}TiO_3$ capacitor with 5 nm Al_2O_3 and the corresponding applied voltages (c). The voltages for the write and read operation are ±15 V and 2 V respectively.

the corresponding capacitance is measured at 2 V with logarithmically distributed time intervals. The initial difference of the capacitance between the high and low state is normalized to unity. At the beginning the capacitance difference is reduced rapidly, but the rate of capacitance change slows down after approximately 100 s. The low state shows a more stable value because its read voltage has the same polarity as the write voltage in this case. The energy band under this condition favors the stabilization of the trapped charge carriers. By extrapolating the lines logarithmically,[14,18] the residual difference between the two states is estimated to be 15% in 1 year and 6% in 10 years. Both values show a promising potential for long-time stability.

2.5. Dielectric Properties at Microwave Frequencies

In order to demonstrate the suitability of the layer structures for microwave components, the BST/Al_2O_3 bilayer capacitors have also been characterized at microwave frequencies. The *CV* measurements are comparable to those carried out at 1 MHz. A clear hysteresis is also induced in the GHz range by the thin Al_2O_3 layer on BST (indicated in Figure S2 in the Supporting Information).

The quality factor (Q) of the BST capacitors, which is an important issue for high frequency applications, is shown in **Figure 7**. The measurements show a typical $1/f$ tendency with increasing frequency both with and without Al_2O_3 layer. When a DC voltage is applied on the sample, the Q factor shows a resonance at $f \approx 2.7$ GHz. This corresponds to an acoustic resonance, which is induced in the BST thin films by electrostriction.[13] There is no significant change in the quality factor for the capacitor with Al_2O_3 layer. As a matter of fact, the Q factor shows a slight improvement, which is explained by the reduced capacitance. This indicates that a bistable capacitor can be made with Al_2O_3 layers in the microwave frequency range without having negative influence on the quality factor.

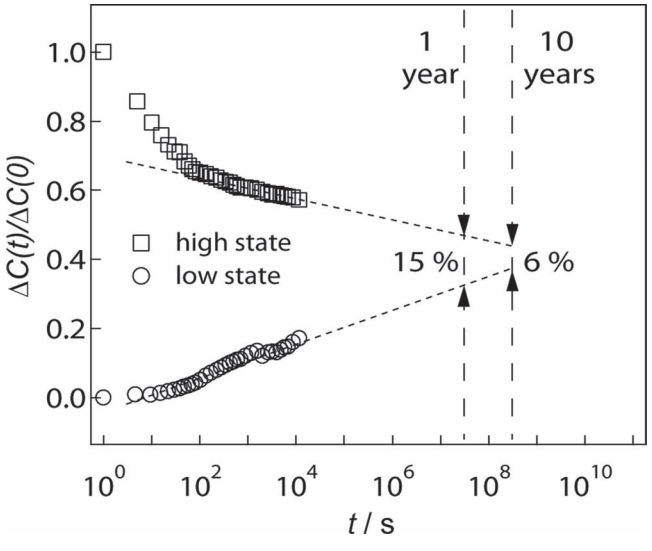

Figure 6. Typical retention characteristics for $d_{Al_2O_3}$ = 5 nm measured at f = 1 MHz. The normalized memory window (i.e., the difference in capacitance between the high and low state) is extrapolated at 1 year and 10 years for room temperature.

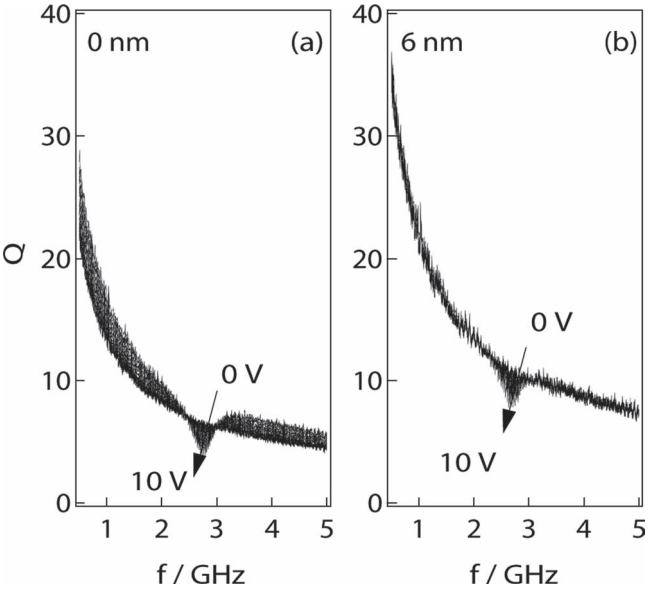

Figure 7. Qf characteristics measured at f = 0.5–5 GHz with DC bias from 0 to ± 10 V for BST capacitors with 0 nm (a) and 6 nm Al_2O_3 (b). The area of the top electrodes is 2.2×10^3 μm².

3. Conclusions

A hysteretic capacitance behavior of non-ferroelectric (Ba,Sr)TiO_3 thin films combined with low permittivity Al_2O_3 barrier layers has been identified by means of capacitance-voltage and capacitance-time measurements. The occurrence of the hysteresis in such system is explained by a mechanism involving ambipolar charge injection through the low permittivity buffer layer and interface charge storage. The BST/Al_2O_3 capacitors show non-volatile capacitance switching, a high flexibility for hysteresis tuning and low insertion loss at microwave frequency, which should enable novel high-frequency devices.

4. Experimental Section

The BST and Al_2O_3 thin films were prepared via RF magnetron sputtering. BST was first deposited onto commercial Si(100)/SiO_2/TiO_2/Pt(111) substrates with an RF power density of 2.5 W cm^{-2} from a 2 inch ceramic target at 650 °C in an Ar/O_2 gas mixture, which contains 1% O_2 at 4Pa total pressure. The nominal target compositions for the samples shown in this article are $Ba_{0.6}Sr_{0.4}TiO_3$ and $Ba_{0.1}Sr_{0.9}TiO_3$, respectively. The compositions of the deposited films were verified with XPS (X-ray photoelectron spectroscopy) and RBS (Rutherford Backscattering Spectrometry) as indicated in the previous work.[7] After BST deposition, the sample was cooled down to room temperature gradually with a rate of 10 K min^{-1} in the deposition atmosphere. Al_2O_3 was deposited onto BST via reactive sputtering from a 2 inch metallic Al target with an RF power density of 2 W cm^{-2} by using a gas mixture of 85% Ar and 15% O_2 at a total pressure of 0.5 Pa. The Al_2O_3 films are fully oxidized under such conditions as confirmed by XPS.[14,20] The deposition rate is about 0.5 nm min^{-1} as determined by the attenuation of Sr 3*d* and Ti 2*p* photoelectron emission after Al_2O_3 deposition.[21] For the dielectric characterization, parallel-plate capacitors with two different electrode geometries were fabricated. For the measurements at 1 MHz the top electrodes were deposited by using a shadow mask with a diameter of 200 μm, whereas photolithography and a lift-off process were employed for the measurement structure used in GHz frequency range.[7] The capacitance measurements were carried out at room temperature at 1 MHz with an Agilent 4294A impedance analyzer and in the GHz range with a Anritsu 37397C network analyzer, respectively.

Supporting Information

Supporting Information is available from the Wiley Online Library or from the author.

Acknowledgements

This work was supported by the German Science Foundation (DFG) in the framework of the Research Training Group (GRK 1037) on Tunable Integrated Components for Microwaves and Optics, TICMO.

Received: February 9, 2012
Revised: April 10, 2012
Published online: July 6, 2012

[1] a) S. Gevorgian, *IEEE Microw. Mag.* **2009**, *10*, 93–98; b) A. K. Tagantsev, V. O. Sherman, K. F. Astafiev, J. Venkatesh, N. Setter, *J. Electroceram.* **2003**, *11*, 5–66; c) P. Bao, T. J. Jackson, X. Wang, M. J. Lancaster, *J. Phys. D: Appl. Phys.* **2008**, *41*, 063001.

[2] a) J. F. Scott, C. A. P. Dearaujo, *Science* **1989**, *246*, 1400–1405; b) R. Waser, *J. Eur. Ceram. Soc.* **1999**, *19*, 655–664.

[3] a) R. Waser, M. Aono, *Nat. Mater.* **2007**, *6*, 833–840; b) R. Waser, R. Dittmann, M. Salinga, M. Wuttig, *Solid State Electron.* **2010**, *54*, 830–840.

[4] a) J. R. Contreras, H. Kohlstedt, U. Poppe, R. Waser, C. Buchal, N. A. Pertsev, *Appl. Phys. Lett.* **2003**, *83*, 4595–4597; b) R. Oligschlaeger, R. Waser, R. Meyer, S. Karthauser, R. Dittmann, *Appl. Phys. Lett.* **2006**, *88*, 042901; c) B. T. Phan, C. Jung, T. Chi, J. Lee, *J. Korean Phys. Soc.* **2007**, *51*, 664–668; d) C. H. Cheng, A. Chin, F. S. Yeh, *IEEE Electr. Device L.* **2010**, *31*, 1020–1022.

[5] a) C. L. Canedy, H. Li, S. P. Alpay, L. Salamanca-Riba, A. L. Roytburd, R. Ramesh, *Appl. Phys. Lett.* **2000**, *77*, 1695–1697; b) H. Li, A. L. Roytburd, S. P. Alpay, T. D. Tran, L. Salamanca-Riba, R. Ramesh, *Appl. Phys. Lett.* **2001**, *78*, 2354–2356; c) L. J. Sinnamon, R. M. Bowman, J. M. Gregg, *Appl. Phys. Lett.* **2002**, *81*, 889–891; d) M. C. Wang, C. C. Tsai, N. C. Wu, K. M. Hung, *J. Appl. Phys.* **2002**, *92*, 2100–2107; e) W. Qin, W. Ai, J. Zhu, J. Xiong, J. Tang, Y. Zhang, Y. Li, *J. Mater. Sci.* **2007**, *42*, 8707–8713; f) T. Kawae, Y. Fukuda, K. Morito, K. Munetomo, A. Morimoto, *Jpn. J. Appl. Phys.* **2009**, *48*, 09KA12.

[6] a) F. M. Pontes, E. R. Leite, E. Longo, J. A. Varela, E. B. Araujo, J. A. Eiras, *Appl. Phys. Lett.* **2000**, *76*, 2433–2435; b) X. Zhu, W. Peng, J. Li, Y. Chen, H. Tian, X. Xu, D. Zheng, *J. Appl. Phys.* **2005**, *97*, 014108; c) X. H. Zhu, W. Peng, H. F. Tian, L. P. Yong, J. Li, J. Q. Li, D. N. Zheng, *J. Phys. D: Appl. Phys.* **2006**, *39*, 4222–4227; d) X. H. Zhu, L. P. Yong, H. F. Tian, W. Peng, J. Q. Li, D. N. Zheng, *J. Phys: Condens. Matter* **2006**, *18*, 4709–4718.

[7] R. Schafranek, A Giere, A. G. Balogh, T. Enza, Y. Zheng, P. Scheele, R. Jakoby, A. Klein, *J. Eur. Ceram. Soc.* **2008**, *29*, 1433–1442.

[8] M. Voigt, A. Bergmaier, G. Dollinger, M. Sokolowski, *J. Vac. Sci. Technol. A* **2009**, *27*, 234–244.

[9] a) C. Basceri, S. K. Streiffer, A. I. Kingon, R. Waser, *J. Appl. Phys.* **1997**, *82*, 2497–2504; b) O. G. Vendik, S. P. Zubko, *J. Appl. Phys.* **1997**, *82*, 4475–4483.

[10] R. Schafranek, S. Payan, M. Maglione, A. Klein, *Phys. Rev. B* **2008**, *77*, 195310.

[11] K. C. Park, J. H. Cho, *Appl. Phys. Lett.* **2000**, *77*, 435–437.

[12] a) A. Q. Jiang, H. J. Lee, G. H. Kim, C. S. Hwang, *Adv. Mater.* **2009**, *21*, 2870–2875; b) A. Q. Jiang, H. J. Lee, C. S. Hwang, T. A. Tang, *Phys. Rev. B* **2009**, *80*, 024119; c) H. J. Lee, G. H. Kim, M. H. Park, A. Q. Jiang, C. S. Hwang, *Appl. Phys. Lett.* **2010**, *96*, 212902; d) H. J. Lee, M. H. Park, Y. J. Kim, C. S. Hwang, J. H. Kim, H. Funakubo, H. Ishiwara, *J. Appl. Phys.* **2011**, *110*, 074111.

[13] A. Giere, R. Schafranek, Y. Zheng, H. Maune, M. Sazegar, R. Jakoby, A. Klein, *Frequenz* **2008**, *62*, 52–56; S. Gevorgian, A. Vorobiev, T. Lewin, *J. Appl. Phys.* **2006**, *99*, 124112.

[14] S. Y. Li, A. Wachau, R. Schafranek, A. Klein, Y. L. Zheng, R. Jakoby, *J. Appl. Phys.* **2010**, *108*, 014113.

[15] a) M. Specht, H. Reisinger, F. Hofmann, T. Schulz, E. Landgraf, R. J. Luyken, W. Roesner, M. Grieb, L. Risch, *Solid State Electron.* **2005**, *49*, 716–720; b) S. Maikap, H. Y. Lee, T. Y. Wang, P. J. Tzeng, C. C. Wang, L. S. Lee, K. C. Liu, J. R. Yang, M. J. Tsai, *Semicond. Sci. Tech.* **2007**, *22*, 884–889; c) S. Nakata, S. Nagai, M. Kumeda, T. Kawae, A. Morimoto, T. Shimizu, *J. Vac. Sci. Technol. B* **2008**, *26*, 1373–1378.

[16] L. Z. Hao, J. Zhu, W. B. Luo, H. Z. Zeng, Y. R. Li, Y. Zhang, *Appl. Phys. Lett.* **2010**, *6*, 032103.

[17] W. K. Shih, E. X.Wang, S. Jallepalli, F. Leon, C. M. Maziar, A. F. Tasch Jr., *Solid State Electron.* **1998**, *42*, 997–1006.

[18] J. H. Jeon, *J. Eur. Ceram. Soc.* **2004**, *24*, 1045–1048.

[19] C. H. Lee, S. H. Hur, Y. C. Shin, J. H. Choi, D. G. Park, K. Kim, *Appl. Phys. Lett.* **2005**, *86*, 152908.

[20] Y. Gassenbauer, A. Wachau, A. Klein, *Phys. Chem. Chem. Phys.* **2009**, *11*, 3049–3054.

[21] K. J. Kim, J. S. Jang, J. H. Lee, Y. J. Jee, C. S. Jun, *Anal. Chem.* **2009**, *81*, 8519–8522.